Interfacial mineral fusion and tubule entanglement as a means to harden a bone augmentation material

Hughes, Erik; Cox, Sophie; Cooke, Megan; Davies, Owen; Williams, Richard; Hall, Thomas; Grover, Liam

DOI:
10.1002/adhm.201701166

ADVANCED HEALTHCARE MATERIALS
www.advhealthmat.de

Interfacial Mineral Fusion and Tubule Entanglement as a Means to Harden a Bone Augmentation Material

*Erik A. B. Hughes, Sophie C. Cox, Megan E. Cooke, Owen G. Davies, Richard L. Williams, Thomas J. Hall, and Liam M. Grover**

A new bone augmenting material is reported, which is formed from calcium-loaded hydrogel-based spheres. On immersion of these spheres in a physiological medium, they become surrounded with a sheath of precipitate, which ruptures due to a build-up in osmotic pressure. This results in the formation of mineral tubes that protrude from the sphere surface. When brought into close contact with one another, these spheres become fused through the entanglement and subsequent interstitial mineralization of the mineral tubules. The tubular calcium phosphate induces the expression of osteogenic genes (runt-related transcription factor 2 (RUNX2), transcription factor SP7 (SP7), collagen type 1 alpha 1 (COL1A1), and bone gamma-carboxyglutamic acid-containing protein (BGLAP)) and promotes the formation of mineral nodules in preosteoblast cultures comparable to an apatitic calcium phosphate phase. Furthermore, alkaline phosphatase (ALP) is significantly upregulated in the presence of tubular materials after 10 d in culture compared with control groups ($p < 0.001$) and sintered apatite ($p < 0.05$). This is the first report of a bioceramic material that is formed in its entirety in situ and is therefore likely to provide a better proxy for biological mineral than other existing synthetic alternatives to bone grafts.

On immersion of calcium-containing hydrogel-based spheres in phosphate rich physiological media, a sheath of precipitate forms around the spheres, which ruptures due to an increase in osmotic pressure. This release of pressure drives the formation of biologically analogous tubular mineral from the gel surface. When spheres are in close proximity to one another, a mechanism of hardening is facilitated by mineral tubules becoming intermeshed, which ultimately causes the spheres to fuse. Formation of the calcium-loaded spheres and their capacity to fill an ex vivo defect in retrieved human bone is reported, in addition to the morphology, structure, and composition of the precipitated mineral phase.

A range of synthetic materials have been developed that are capable of filling hard tissue defects to overcome the issues that are often associated with autologous tissue harvesting, such as local tissue morbidity and lack of availability.[1,2] In particular, there have been many ceramic-based materials used for hard tissue augmentation. Calcium phosphate- and calcium sulfate-based products are available commercially, but are yet to replace autograft as the so-called "gold-standard."[3,4] The ceramic materials used for the augmentation of hard tissues are often produced using high-temperature treatment processes, meaning that they are of high crystallinity and relatively low specific surface area.[5–7] Consequently, synthetic ceramic bone replacements often bear little resemblance to native bone mineral, which is predominantly nanocrystalline hydroxyapatite (HA, $Ca_5(PO_4)_3OH$) that is poorly crystalline.[8] Even in the case of cements, which harden through reprecipitation in the body, much of the hardened structure is formed in the presence of excess microcrystalline reactant.[9,10] Moreover, many conventional regenerative materials are absent of channels to support the penetration of surrounding vascular networks.[11,12] The level of structuring that is possible with synthetic alternatives to bone graft is limited to the production of biomimetic corals and sponge-like structures that provide an interporous network for bone regeneration, but replicate none of the microstructural organization of hard tissue at the osteonal level.[13–15] Hard tissues exhibit precisely defined hierarchical architectures, with organization from the molecular level through to the macroscale. It is this well-preserved architecture that is critical to the extraordinary mechanical performance of bone, which is stronger and tougher per unit weight than steel.[13] Adopting bioinspired approaches to design biomaterials may further enable the generation of regenerative materials with advanced capabilities of function and cellular interaction.[16,17]

One preserved feature of hard tissue is the presence of intricate tubular networks, such as canaliculi, Haversian canals, and Volkmann's canals found in mature bone, as well as dentinal tubules within teeth, that are critical to the function of such tissues.[18–20]

Dr. E. A. B. Hughes, Dr. S. C. Cox, M. E. Cooke, Dr. O. G. Davies, Dr. R. L. Williams, T. J. Hall, Prof. L. M. Grover
School of Chemical Engineering
University of Birmingham
Birmingham B15 2TT, UK
E-mail: l.m.grover@bham.ac.uk
M. E. Cooke
Institute of Inflammation and Ageing
MRC Musculoskeletal Ageing Centre
QE Hospital
B15 2TT, UK
Dr. O. G. Davies
School of Sport, Exercise and Health Sciences
Loughborough University
Loughborough LE11 3TU, UK

DOI: 10.1002/adhm.201701166

Tubular channels like these are essential for transporting chemicals, gases, and nutrients in order to maintain the viability of cells cocooned within typically dense mineralized tissue. Mimicking the natural structural features of bone is a major challenge but one that is subject to substantial research effort. A prerequisite to facilitating the development of vascular networks throughout hard tissue scaffolds may be the provision of tubular structures similar in nature to those found in mineralized tissues. It has been shown that mineralized tubular frameworks provide an ideal framework to mediate revascularization of bone in vivo.[21]

Mineral tubes similar to those found in bone and teeth may be formed using a system that is analogous to a chemical garden, where hollow tubular precipitates form at the interface between a cationic seed crystal and an anionic solution.[22,23] These structures have been likened to a range of tubular minerals found throughout nature.[24,25] Surprisingly, there is relatively little work that examines the use of such systems for biotechnology applications despite the fact that tubes have been shown to support the entrapment and growth of cells.[26,27] With the exception of calcium silicates, phosphates, and carbonates, the majority of salts traditionally generated in chemical gardens would not be compatible with implantation into the body, including but not limited to cobalt, copper, iron, manganese, and nickel compounds.[22–24,26,28] There has recently been work that has shown that it is possible to produce biologically relevant calcium phosphate structures at the interface between a cation-loaded hydrogel and anionic solution.[29–32] Indeed, we recently reported on the formation of tubular calcium phosphate that resembles tubular architectures found in bone both structurally and compositionally.[32] The generation of these structures results from the exposure of calcium-loaded agarose layered with a phosphate rich solution, which ultimately produces a forest of hollow white precipitate tubes (**Figure 1**a). Initially, a precipitate is formed at the gel–liquid interface, which impedes diffusion and creates an

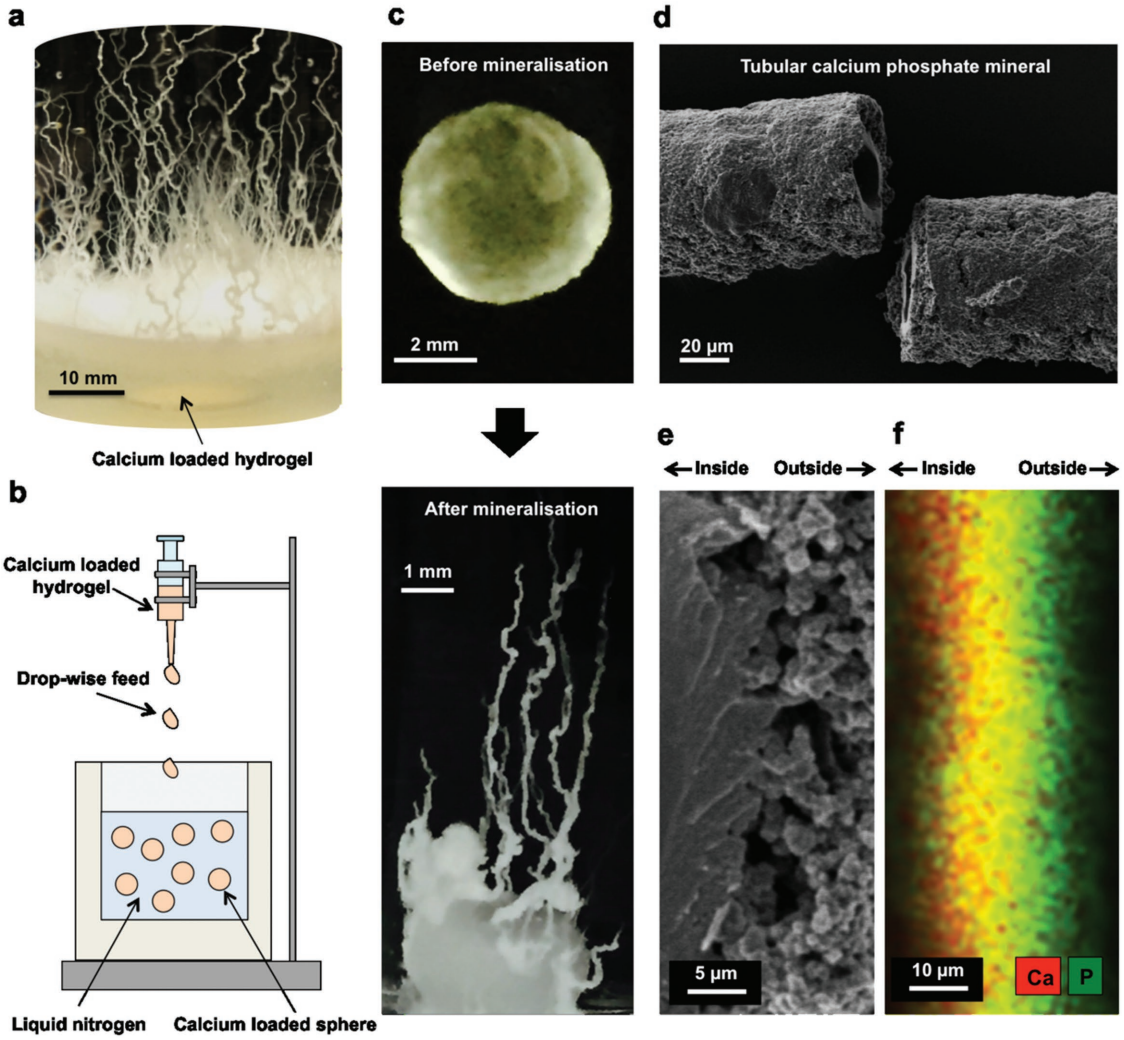

Figure 1. a) Conventional experimental set-up we previously reported in ref. [32], which produces calcium phosphate tubules that are structurally and compositionally similar to microstructures within bone, providing the starting point for the work reported herein. b) Schematic of fabrication method of calcium-loaded spheres, involving drop-wise addition of calcium-loaded agarose hydrogel into a reservoir of liquid nitrogen. c) Calcium-loaded spheres before and after mineralization, showing the ejection of tubular calcium phosphate mineral. d) SEM micrograph showing the tubule microstructure, consisting of a bilayer tubule wall surrounding a hollow core. e) SEM micrograph of tube wall bilayer structuring. f) µ-XRF elemental mapping of a calcium phosphate tubule cross section (Kα channels for calcium (red) and phosphorous (green) shown).

osmotic pressure. When the osmotic pressure causes localized rupture of the precipitate layer, calcium ions are able to diffuse into the liquid phase where a tubular calcium phosphate-based precipitate forms.[32,33] Growth of these tubes is maintained through cyclic build-ups in osmotic pressure and release, which drives calcium ions through the established tubule to the tip where it ruptures, and a new section of tubule is formed.[32,33] The mineral from which these tubules are formed is of low crystallinity calcium phosphate, similar to that found in the body.

The tubular precipitate did not only form on planar surfaces, but also formed when spheres of hydrogel prepared with a 1 M calcium nitrate solution were placed into a 0.5 M phosphate-augmented physiological solution. The spheres were produced through the drop-wise addition of hot (80–90 °C) calcium-loaded agarose gel mixture through a 2 mm wide pipette aperture into a reservoir of liquid nitrogen (Figure 1b). Upon contact with the liquid nitrogen, the gel droplets quickly solidify as spheres through the inverse Leidenfrost effect.[34] The resulting particles were of average diameter 3.7 ± 0.4 mm (mean of $n = 10$ ± standard deviation (SD)). The use of this method of manufacture meant that we were able to produce spherical agarose particles that were loaded with relatively high concentrations of calcium ions (>1 M), which would be very difficult to achieve using standard processing methods or if soaking preformed spheres in cation-containing solutions.[35] Agarose was selected as the soft material of choice as a consequence of its neutral charge, meaning that it does not impede diffusion of the calcium ions. Others have reported the use of mineralized hydrogel, including agarose-based systems, for bone augmentation.[36–40] The novelty of the system described in this paper is the ability to generate biologically analogous calcium phosphate structures that aid in hardening an osteogenic bone graft material in situ.

When the calcium-loaded spheres were immersed in phosphate solutions, tubules precipitated around the periphery of the particles but grow preferentially upward due to buoyancy effects (Figure 1c).[23] Altering the metal and reactive counter ion concentrations directly influences the kinetic driving forces of tubular self-assembly, including osmotic, diffusion, and pH gradients that exist within the material system. This influences the gross morphology of the tubes and can also be used to adjust formation rate. Increasing phosphate solution concentration from 500×10^{-3} M to 1 M allows control over mineral tubular growth rate between 0.3 mm min^{-1} (18 mm h^{-1}) to 0.5 mm min^{-1} (30 mm h^{-1}) (Figure S1, Supporting Information).

Scanning electron microscopy (SEM) images show that the tubules typically exhibit diameters between 100 and 150 µm, which is ideal for ingress of osteogenic cells (Figure 1d).[41] Additionally, these channels facilitate mass transport of ionic solute during structure formation, similar to how osteon structures direct the flow of blood within Haversian systems in order to exchange nutrients and gases. They also exhibit a hierarchical bilayer wall structure comprised of low crystallinity HA ($Ca_5(PO_4)_3OH$) and dicalcium phosphate dihydrate ($CaHPO_4 \cdot 2H_2O$) (Figure 1e; Figure S2, Supporting Information). This structure develops inwards as a consequence of the contrasting environments inside and outside of the tube resulting in a steep concentration gradient of reactive species across the tube wall. This ultimately results in a calcium rich inner wall and phosphate rich outer wall (Figure 1f).[42]

Mineralizing calcium-loaded spheres placed in close contact with one another fuse through the formation of precipitate and the development of interweaving tubes at their periphery (**Figure 2**a). The interactions formed between the spheres were of sufficient strength to allow for the fusion of multiple spheres to form a larger structure (Movie S1, Supporting Information). Elemental mapping using micro X-ray fluorescence (µ-XRF) confirmed that the particles were united by a calcium phosphate phase (Figure 2b). It was possible to assemble the gel spheres into relatively complex geometries, such as the pyramid shown in Figure 2c. 3D microcomputed tomography (µ-CT) reconstructions of this structure show that mineral coverage (red and green) occurs extensively across the surfaces of hydrogel spheres (blue), and even in the center of the structure (Figure 2d). Mechanical properties of hardened cylindrical structures (12 mm high by 12 mm wide) were assessed under compressive loading to ascertain the adhesion between the spheres of a mineralized construct. Structures possessed a compressive strength of 200 ± 40 kPa (mean of $n = 3$ ± SD). Although the interfacial precipitate that develops between spheres is able to support the formation of mineralized constructs, subsequent failure of these structures under relatively low forces suggests application in the treatment of low-load bearing defects, such as that of the craniofacial skeleton. Despite the low resistance of mineralized spheres to load, within an augmented defect space the integrity of a hardened network of spheres will likely be supported by adjacent hard tissue. Furthermore, the strength of the graft may be improved over time by the ingress of newly forming bone between spherical structures and the integration of tubules with native bone interfaces.

To demonstrate that this approach could be used for the augmentation of a hard tissue defect, a cylindrical defect ≈10 mm wide and 15 mm deep was introduced into an ex vivo human tissue sample, which was then packed with calcium-loaded spheres (**Figure 3**a). The filled defect was then placed into a phosphate rich medium (1 M phosphate solution), and mineral was observed to form rapidly across the surface with the formation of tubes becoming apparent soon thereafter. After 24 h, this structure could be inverted and irrigated with water without a loss of mechanical integrity (Movie S2, Supporting Information). µ-CT revealed the extent of mineral deposition within the defect (Figure 3b). Cross-sectional images show mineral around the surface of spheres and tubular structures within the defect, filling the interparticulate spaces with a mineral phase. From µ-CT examination, the interfaces between the spheres and the mineral deposited are extremely difficult to differentiate from the opposing bone. µ-XRF analysis demonstrates that the elemental composition of precipitated calcium phosphate mineral is similar to the surrounding tissue, also making it difficult to distinguish a clear interface between bone and the spheres. It is likely that compositional similarities between mineral phases aid the bone bonding capability of the system at the interface between bone tissue and mineral releasing spheres (Figure 3c; Figure S3, Supporting Information).

In order to demonstrate the biocompatibility of tubular precipitate and assess its osteoinductive properties, we analyzed its capacity to induce osteogenesis within a population of murine MC3T3 preosteoblasts. Our findings were compared with a synthetic HA phase that had undergone a sintering treatment

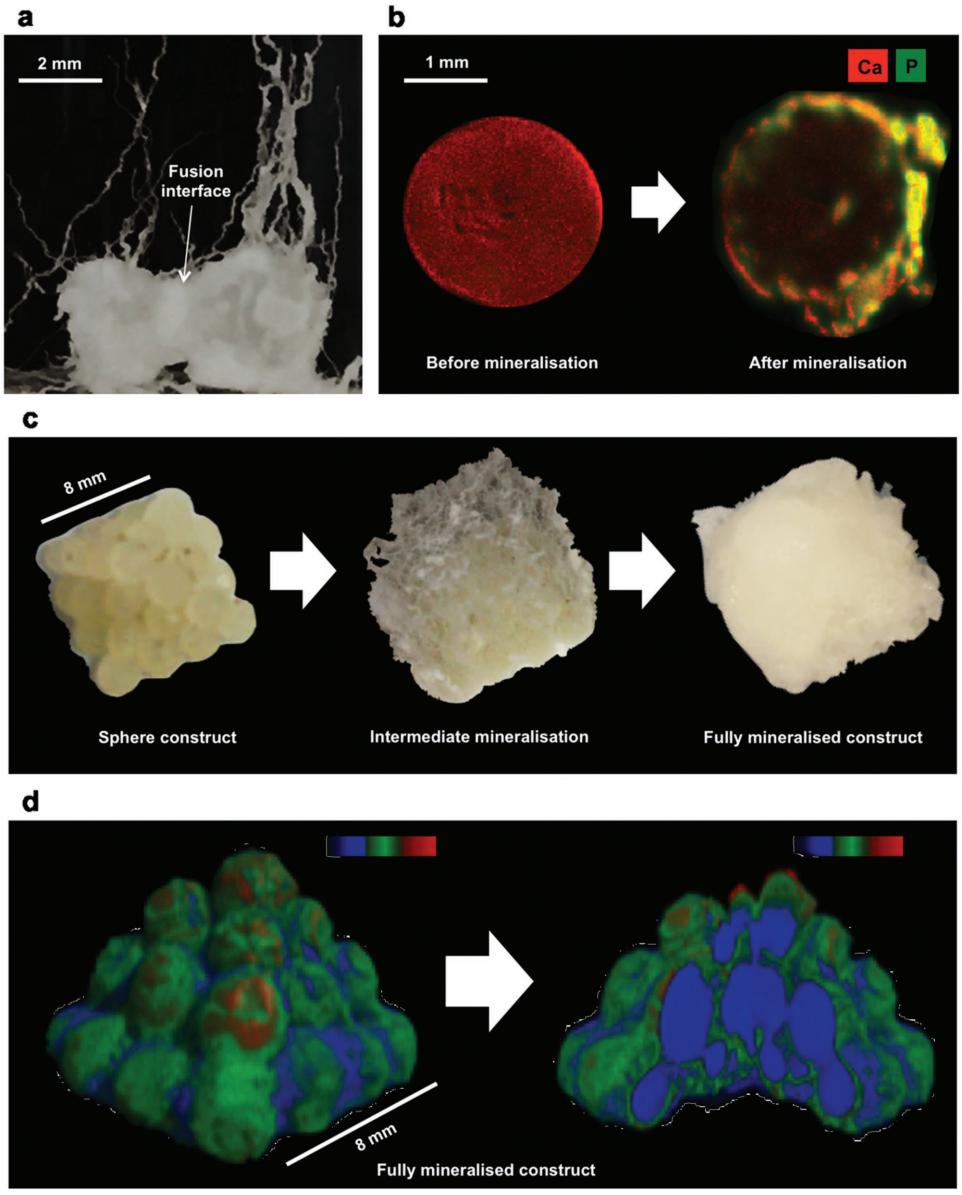

Figure 2. a) Fusion of two calcium-loaded spheres in close proximity to one another during mineralization. b) μ-XRF elemental mapping of a calcium-loaded sphere cross-section before and after inducing mineralization (Kα channels for calcium (red) and phosphorous (green) shown). c) Calcium-loaded sphere pyramid construct before and after triggering mineralization, leading to complete unification. d) μ-CT of calcium-loaded sphere pyramid after submersion in phosphate solution. Color scales in-set represent an increase in relative density of material from blue (calcium-loaded sphere) to green and red (mineral).

(HA). Similar phases are routinely applied as bone grafts, and therefore provided an osteogenic control within this study.[5–7]

The biological response of MC3T3 cells to tubular mineral was examined using a transwell culture system in which our calcium phosphate tubes were distributed within an insert chamber, and the indirect effects were monitored. Cell viability assessed using calcein AM/propidium iodide staining demonstrated that tubular mineral exhibited no adverse cytotoxic effects over a period of 10 d (**Figure 4**a). This was further confirmed by alamar blue, which overall identified comparable levels of metabolic activity in line with both positive and negative controls, as well as the HA standard (Figure 4b).

In order to examine the comparative osteoinductive effects of tubes, we analyzed levels of alkaline phosphatase (ALP) activity in each culture at 3, 7, and 10 d time points (Figure 4c). Levels of ALP generally increased for all treatments over a period of 10 d in culture. At day 3, ALP generated by cells in pro-osteogenic media and HA groups was significantly increased ($p < 0.001$) compared with negative control and Tube groups, albeit at relatively low levels. ALP was found to be significantly ($p < 0.001$) upregulated in the positive osteogenic control at day 7 when compared with both HA and Tube groups, which is likely related to the availability of free phosphates (exogenous β-glycerophosphate) for cells to utilize within these

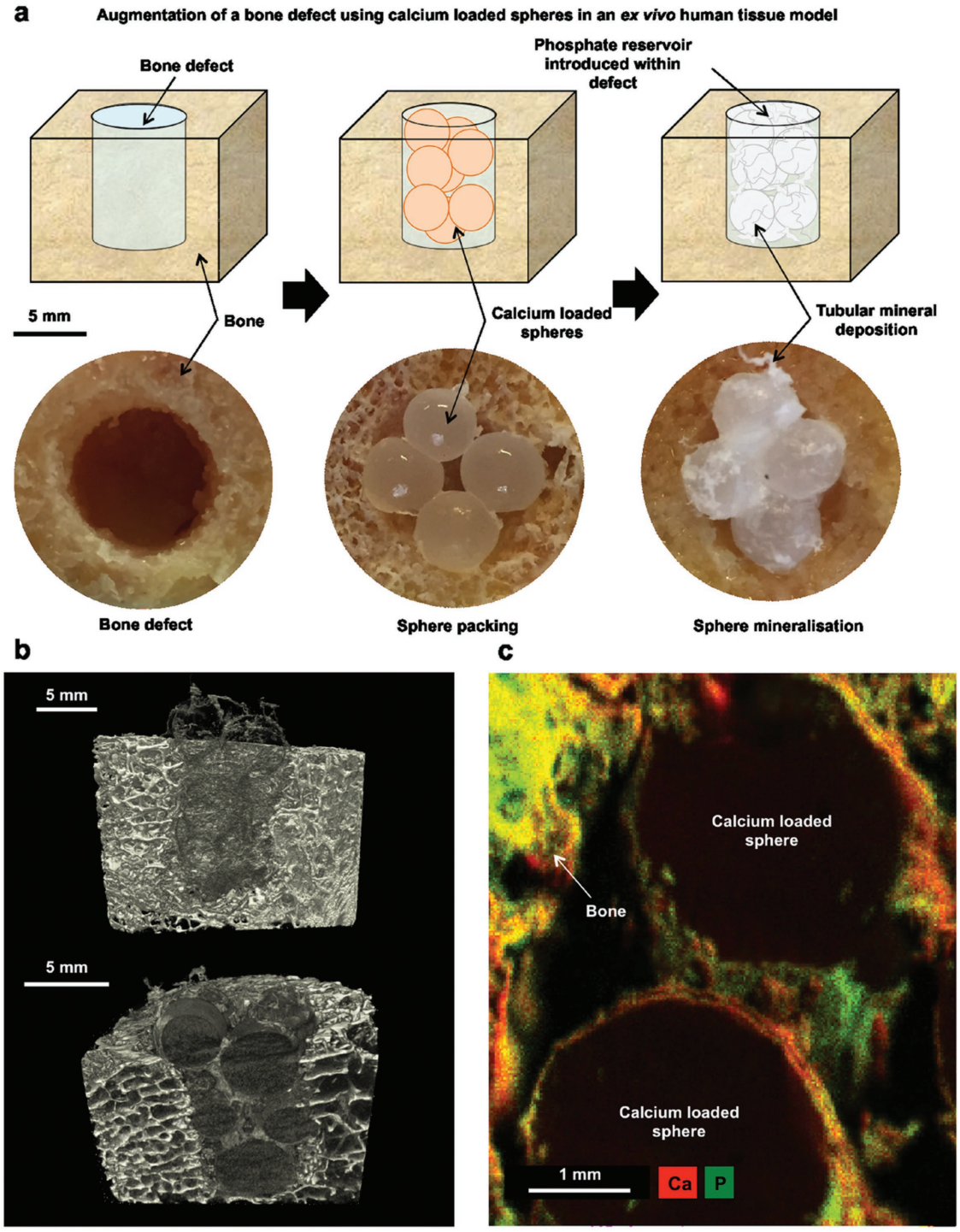

Figure 3. a) Schematic of calcium-loaded spheres augmenting an ex vivo human bone defect, showing an empty bone defect, the packing of spheres to augment the defect, and triggering of mineralization with 1 M phosphate solution. b) μ-CT of human hard tissue model containing mineralized calcium-loaded spheres that have deposited mineral and tubular structures within the defect. c) μ-XRF elemental mapping of a cross-section of the human hard tissue defect (Kα channels for calcium (red) and phosphate (green) shown).

particular control groups. However, by day 10, ALP activity was significantly upregulated in the Tube group compared with the negative control ($p < 0.001$), positive control ($p < 0.001$), and sintered HA groups ($p < 0.05$). Detection of significantly enhanced levels of ALP in the Tube groups suggests that even in an early stage of in vitro culture, tubular calcium phosphate is able to facilitate favorable conditions for osteogenic differentiation more so than synthetic HA.

The relative osteoinductive effects of tubular mineral were further determined using quantitative real-time polymerase

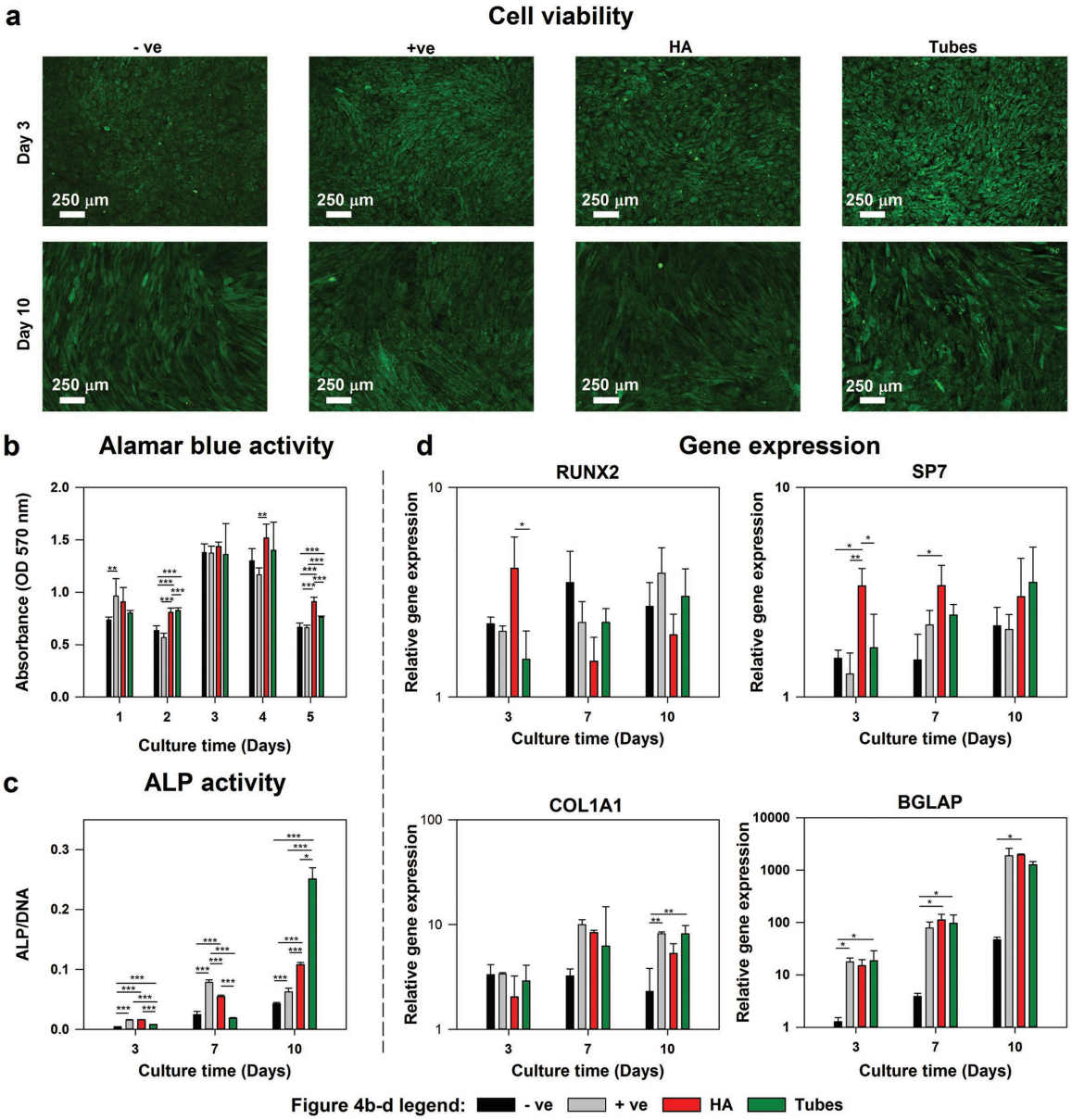

chain reaction (qRT-PCR) to reveal the expression of genetic markers for both immature and mature osteoblasts (Figure 4d). The expression of early osteogenic markers runt-related transcription factor 2 (RUNX2) and transcription factor SP7 (SP7) were in line with the osteogenic control. RUNX2 and SP7 were significantly reduced in the Tube group at day 3 when compared with HA ($p = 0.033$; $p = 0.024$, respectively), possibly indicating an earlier primary osteogenic response in this culture. The expression of collagen type 1 alpha 1 (COL1A1) was upregulated in all treatments compared with the negative control but not significant between treatments, which indicates that the rate of extracellular matrix (ECM) deposition is not negatively affected following exposure to calcium phosphate tubes. Similarly, expression of the mature osteoblast marker bone gamma-carboxyglutamic acid-containing protein (BGLAP) are comparable between preosteoblasts exposed to tubular precipitate, HA and the osteogenic control over a period of 10 d in culture.

Formation of comparable calcified nodules was observed at day 10 in all cultures, as shown by alizarin red staining. Nodules formed in the presence of tubes were comparable to those observed in the presence of HA (Figure 4e). Collectively, these results demonstrate that tubular calcium phosphate mineral generated by calcium-loaded hydrogel spheres in the present study is biocompatible and exhibits an osteoinductive profile consistent with a clinically applied calcium phosphate, such as sintered HA. Further work will need to be conducted to determine the osteoconductive topographic effects of the tubular structures to comprehensively define its efficacy as a scaffold for hard tissue repair.

Inspired by processes that are able to mimic the generation of natural tubular mineral structures, we have developed a device capable of augmenting a hard tissue defect through the production of tubular mineral. The material consists of calcium-loaded spheres manufactured using a process that allows for the incorporation of high concentrations of calcium. Immersion of these spheres in physiologically relevant solutions rich in phosphate stimulates tube formation, which means that they could be ideal for use in biological environments. Compared with the majority of synthetic bone substitutes that are typically dense and highly crystalline, this system enables (1) the formation of tubular calcium phosphate mineral that is structurally and compositionally akin to the tubular features found in bone and tooth, providing a structured osteogenic scaffold, (2) mineral formation in situ in the absence of microcrystalline reactant, facilitating a low crystallinity product comparable to the surrounding hard tissue, and (3) tunable mineral synthesis by the adjustment of precipitation parameters, enabling physical properties such as fusion time to be modified using physiologically relevant conditions, such as phosphate solution concentrations. The microscale structural features of the mineral phase may also enable better vascularization of the implant.[21]

In summary, we present a strategy for directly delivering hierarchical tubular mineral into hard tissue defects using spheres of agarose hydrogel loaded with calcium. In phosphate solutions, these spherical structures fuse, forming a solid through the intermeshing of mineral tubules that are expelled from the surface of the soft material.

Experimental Section

Calcium-Loaded Hydrogel Fabrication and Mineral Initiation: Calcium-loaded gels were made by adding 5 wt% agar powder (for microbiology, Sigma-Aldrich, UK) to 1 M calcium solutions prepared from calcium nitrate tetrahydrate crystals (99%, ACS reagent, Sigma-Aldrich, UK) and distilled water before heating the mixture to 80–90 °C. For conventional set-up, a layer of gel was set in clear cylindrical containers and allowed to cool to room temperature. For calcium-loaded spheres, warm gel was added drop-wise to an insulated chamber of liquid nitrogen. Spheres were collected after dissipation of the nitrogen. Mineralization was initiated upon gel surfaces, calcium-loaded sphere constructs, and within an ex vivo bone defect using phosphate solutions prepared by dissolving crystals of dibasic ammonium phosphate (≥98.0%, reagent grade, Sigma-Aldrich, UK) at concentrations between 500×10^{-3} M and 1 M.

Compressive Strength Testing of Mineralized Constructs: Calcium-loaded hydrogel spheres containing 1 M calcium ions were packed into a 12 × 12 mm cylinders. Mineralization was initiated by submerging the constructs in 1 M dibasic ammonium phosphate solution, and the hardened structures were recovered after 24 h. Mechanical data was collected using a Zwick/Roell Z030 universal tester equipped with a 100 N load cell. Compression tests were performed at a speed of 1 mm min^{-1}, until failure of the specimens. The maximum force to failure was noted and used to calculate the compressive strength with Equation (1)

$$\sigma = F/A \tag{1}$$

where σ is compressive strength (MPa), F is force (N), and A is contact area (mm^2).

Units of compressive strength were subsequently converted from MPa to kPa thereafter.

SEM: Samples were placed on an aluminum stub using double-sided sticky carbon discs. Gold sputter coating was performed prior to imaging using a K550X sputter coater (Quorum Technologies, UK). SEM images were then acquired using an EVO MA 10 scanning electron microscope (Carl Zeiss AG, Germany).

μ-XRF: Specimens were elementally mapped using an M4 Tornado instrument (Bruker, USA). Measurement settings of 20 ms $pixel^{-1}$ over 25 frames in the case of Figures 1f and 2 frames in the case of Figures 2b and 3C, were employed with the instrument operating at 50 kV with anode current of 300 mA. During measurements, the chamber was maintained at 500 mbar in case of Figure 1f.

Human Tissue Model: Bone tissue was collected from patients undergoing elective knee replacement surgery. The United Kingdom

Figure 4. a) Fluorescent microscope images of cells stained with calcein AM and propidium iodide, showing viable cells (green) and dead cells (red). MC3T3 cells were cultured either in supplemented media (negative control group = –ve) or supplemented osteogenic media (positive control group = +ve), and additionally in supplemented media in the presence of synthetic HA that had been sintered (HA), as well as tubular calcium phosphate (Tubes). For reference, these groups correspond to the remaining parts of this figure as indicated. b) Metabolic activity of MC3T3 cells as determined by alamar blue (mean of $n = 6 \pm$ SD). c) Detection of ALP produced by MC3T3 cells (mean of $n = 3 \pm$ SD). d) Corresponding gene expression of RUNX2, SP7, COL1A1, and BGLAP determined by qRT-PCR (mean of $n = 3 \pm$ SD). For panels (b–d), significant difference found by one-way ANOVA and post-hoc statistical testing analysis is indicated by *, **, and ***, which correspond to p values of $p < 0.05$, $p < 0.01$, and $p < 0.001$, respectively. e) Optical microscopy of cultures fixed and stained with alizarin red showing the formation of comparable mineral nodules in the presence of osteogenic media, HA and Tube groups after 10 d.

National Research Ethics Service (East of Scotland Research Ethics Service) provided ethical approval (11/ES/1044). Tissues were washed using phosphate buffered saline (PBS) (calcium and magnesium free, Sigma-Aldrich, UK) before defects 10 mm wide and a minimum of 10 mm deep were introduced using a surgical drill. Calcium-loaded spheres were gently packed into defect spaces and mineralization initiated as detailed above.

CT Scanning: Samples were transferred to a sealed low X-ray attenuation tube. Structures were scanned using a Skyscan1172 µ-CT instrument (Bruker, USA) with 60 kV maximum X-ray energy, 6 W beam power, 2000 ms exposure per projection, and 12.44 µm pixel size. Slice data was reconstructed using NRecon (Version 1.6.10, Bruker) and visualized using CTVox (Version 3.0, Bruker). For mineralizing sphere pyramid constructs, grayscale images were artificially colored by assigning blue, green, and red transfer functions to grayscale ranges matching the calcium-loaded spheres (blue) and mineralized regions (green and red). For the mineralized human defect model, an opacity transfer function was applied to best segment the grayscale range corresponding to the tubules from the rest of the structure to render 3D images of deposited mineral within the defect.

Synthesis of Synthetic Hydroxyapatite and Sintering Procedure: HA was prepared by sol–gel precipitation following a reported method.[43] For sintering, powder was transferred to a heatproof ceramic dish and subjected to 650 °C for 3 h in a CWF 1300 furnace (Carbolite, UK). The heating and cooling ramp rate was set at 5 °C min^{-1}, and sintered HA powder (HA) was recovered only after the furnace had returned to room temperature.

In Vitro Cell Culture: MC3T3 murine preosteoblast cells were purchased from America Type Culture Collection (ATCC) and used between passages 4 and 6. Cells were initially cultured in growth medium consisting of alpha-modified Minimum Essential Medium supplemented with 10% fetal bovine serum (FBS), 2.4% L-glutamine, and 1% penicillin/streptomycin. Osteogenic medium was further supplemented with 10×10^{-3} M β-glycerophosphate, 50 µg mL^{-1} L-ascorbic acid, and 10×10^{-9} M dexamethasone (Sigma-Aldrich, UK).

Cell Viability: Viability was assessed at days 3 and 10. Cell cultures were immersed in 1 mL growth medium supplemented with 3×10^{-6} M calcein acetoxymethyl ester (Calcein AM, Life Technologies, UK) and 1×10^{-6} M propidium iodide (Life Technologies, UK) and incubated at 37 °C for 5 min. Cell viability was determined visually using an Olympus IX81 fluorescence microscopy (Olympus, USA).

Alamar Blue Metabolic Activity: MC3T3s were seeded at a density of 6.5×10^3 cells cm^{-2} in growth medium and allowed to adhere at 37 °C for a period of 24 h. Following 24 h culture transwell inserts (0.4 µm ThinCert, Greiner Bio-One, Austria) containing 20 mg sintered HA or 20 mg tubular precipitate (Tubes) were incorporated and the total media volume adjusted to 2 mL. Metabolic activity was assessed at every 24 h over a total period of 5 d by incorporating 10% Alamar Blue reagent (Life Technologies, UK) into the cell culture medium and measuring absorbance at 570 nm using a Synergy HT microplate reader (Biotek, UK).

ALP Activity: Cellular ALP activity was quantified using the SensoLyte pNPP ALP Assay Kit (AnaSpec, USA). MC3T3s were plated in 12-well plates at an initial seeding density of 26×10^3 cells cm^{-2} in the presence of 1 mL growth medium. Following 24 h culture transwell inserts (0.4 µm ThinCert, Greiner Bio-One, Austria) containing 20 mg sintered HA or 20 mg tubular HA (Tubes) were incorporated and the total media volume adjusted to 2 mL. ALP activity was measured at 3, 7, and 10 d according to the manufacturer's instructions. Briefly, cell monolayers were washed twice using 1× assay buffer provided. Cells were detached from the surface of the culture plate in the presence of 200 µL permeabilization buffer using a cell scraper. The resulting cell suspension was collected in a microcentrifuge tube, incubated at 4 °C for 10 min under agitation, and then centrifuged at 2500 g for 10 min. Supernatant was transferred to a 96-well plate where it was combined with an equal volume of pNPP substrate. Absorbance was measured at 405 nm using a Synergy HT microplate reader (Biotek, UK). ALP activity was normalized to DNA concentration (see the "DNA isolation" section).

RNA Isolation and qRT-PCR: Following culture, total RNA was isolated using TRIzol reagent (LifeTechnologies, UK); the manufacturer's instructions were followed. Briefly, TRIzol reagent was used to directly lyse cells before chloroform (Sigma Aldrich, UK) was added to separate the aqueous RNA phase through centrifugation. The RNA phase was removed and isopropanol (Fisher Scientific, UK) was added to precipitate the RNA. The precipitate was centrifuged and then washed with 75% ethanol prepared from absolute (Fisher Scientific, UK) before drying in a vacuum desiccator. Finally, the pellet was resuspended in molecular biology grade water (Fisher Scientific, UK). RNA concentration and A260/280 ratio were measured using a spectrophotometer (NanoDrop 2000, ThermoScientific).

QuantiFast one-step master mix (Qiagen) was used to measure mRNA expression of RUNX2, SP7, COL1A1, BGLAP, and β-actin, which was used as a housekeeping gene. All primer sequences were designed by KiCqStart and supplied by Sigma-Aldrich (Gillingham, UK); forward and reverse sequences are shown in Table S1 in the Supporting Information. qRT-PCR was performed using a BioRad CFX384 (BioRad, USA), and relative expression was calculated using ddCT, normalized to β-actin.

DNA Isolation: DNA was purified from interphase and organic phase components collected during RNA isolation following removal of the RNA phase (see *RNA Isolation and qRT-PCR* of methods section). Briefly, absolute ethanol was added to the mixtures, which were incubated for 3 min, before centrifugation to pellet the DNA. DNA was washed twice by resuspending the pellet in 0.1 M sodium citrate (Sigma Aldrich, UK) solution prepared with 90% molecular grade water and 10% ethanol, incubating for 30 min, and centrifugation at 2000 × *g* for 5 min at 4 °C. DNA was then resuspended in a 75% ethanol and 25% molecular water solution, incubated for 20 min before being centrifuged, and the pellet air dried for 10 min following removal of the supernatant. Finally, the pellet was resuspended in 8×10^{-3} M NaOH solution prepared with molecular grade water, and the DNA concentration and A260/280 ratio measured using a spectrophotometer (NanoDrop 2000, ThermoScientific). ALP activity was normalized to the DNA concentration.

Alizarin Red Calcium Staining: Cultures were washed using sterile PBS and subsequently fixed with 4% paraformaldehyde for 20 min at room temperature. 40×10^{-9} M alizarin red solution (Sigma-Aldrich, UK), which had been adjusted to pH 4.2 using ammonium hydroxide was applied to each culture for a period of 20 min. Unbound stain was eluted by successive washes in PBS. Images were captured using an INVERSO TC100 inverted microscope (Resolution, UK) at 10× magnification.

Statistical Analysis: All statistically analysis was performed using SigmaPlot 13.0 software. All groups underwent normality testing by Shapiro–Wilk method and equal variance testing by Brown–Forsythe method. One-way analysis of variance (ANOVA) was used to determine if statistical differences existed between sample groups at different time points, with alpha level of 0.05. Post-hoc all pairwise multiple comparison tests were performed using the Holm–Sidak method. Values of $p < 0.05$ were deemed to be significant.

Supporting Information

Supporting Information is available from the Wiley Online Library or from the author.

Acknowledgements

All authors contributed equally to this work. E.H., R.W., and L.G. developed the device concept discussed herein. E.H. and T.H. fabricated calcium-loaded spheres using liquid nitrogen method described. E.H., M.C., and L.G. developed the ex vivo human bone defect model. E.H. and S.C. performed µ-CT scanning. E.H. and O.D. undertook in vitro biological experiments. E.H., O.D., and M.C. performed qRT-PCR analysis. The authors thank the financial support provided by the EPSRC

(project number 1294393 – medical materials) undertaken in association with TWI Ltd.

Conflict of Interest

The authors declare no conflict of interest.

Keywords

bone augmentation, hard tissue defect model, mineralization, tubular mineral

Received: October 2, 2017
Revised: November 8, 2017
Published online: January 11, 2018

[1] R. F. LaPrade, J. C. Botker, *Arthroscopy* **2004**, *20*, e69.
[2] G. M. Calori, M. Colombo, E. L. Mazza, S. Mazzola, E. Malagoli, G. V. Mineo, *Injury* **2014**, *45*, 116.
[3] S. V. Dorozhkin, *Ceram. Int.* **2015**, *41*, 13913.
[4] H. Shegarfi, O. Reikeras, *J. Orthop. Surg.* **2009**, *17*, 206.
[5] A. B. Hazar Yoruç, A. Karakaş, A. Koyun, T. Yildiz, *Acta Phys. Pol., A* **2012**, *121*, 233.
[6] A. L. Giraldo-Betancur, D. G. Espinosa-Arbelaez, A. d. Real-López, B. M. Millan-Malo, E. M. Rivera-Muñoz, E. Gutierrez-Cortez, P. Pineda-Gomez, S. Jimenez-Sandoval, M. E. Rodriguez-García, *Curr. Appl. Phys.* **2013**, *13*, 1383.
[7] M. Prakasam, J. Locs, K. Salma-Ancane, D. Loca, A. Largeteau, L. Berzina-Cimdina, *J. Funct. Biomater.* **2015**, *6*, 1099.
[8] W. Querido, A. L. Rossi, A. P. C. Campos, A. M. Rossi, M. Farina, *Mater. Res.* **2013**, *16*, 970.
[9] T. J. Brunner, R. N. Grass, M. Bohner, W. J. Stark, *J. Mater. Chem.* **2007**, *17*, 4072.
[10] L. C. Chow, *Dent. Mater. J.* **2009**, *28*, 1.
[11] M. Lovett, K. Lee, A. Edwards, D. L. Kaplan, *Tissue Eng., Part B* **2009**, *15*, 353.
[12] L. H. Nguyen, N. Annabi, M. Nikkhah, H. Bae, L. Binan, S. Park, Y. Kang, Y. Yang, A. Khademhosseini, *Tissue Eng., Part B* **2012**, *18*, 363.
[13] U. G. K. Wegst, H. Bai, E. Saiz, A. P. Tomsia, R. O. Ritchie, *Nat. Mater.* **2014**, *14*, 23.
[14] D. W. Green, W. F. Lai, H. S. Jung, *Mar. Drugs* **2014**, *12*, 2877.
[15] D. W. Green, B. Ben-Nissan, K. S. Yoon, B. Milthorpe, H. S. Jung, *Trends Biotechnol.* **2017**, *35*, 43.
[16] P. Yu, C. Ning, Y. Zhang, G. Tan, Z. Lin, S. Liu, X. Wang, H. Yang, K. Li, X. Yi, Y. Zhu, C. Mao, *Theranostics* **2017**, *7*, 3387.
[17] M. Yang, Y. Shuai, C. Zhang, Y. Chen, L. Zhu, C. Mao, H. OuYang, *Biomacromolecules* **2014**, *15*, 1185.
[18] D. M. Cooper, C. D. Thomas, J. G. Clement, A. L. Turinsky, C. W. Sensen, B. Hallgrimsson, *Bone* **2007**, *40*, 957.
[19] I. S. Maggiano, C. M. Maggiano, J. G. Clement, C. D. L. Thomas, Y. Carter, D. M. L. Cooper, *J. Anat.* **2016**, *228*, 719.
[20] J. Jowsey, *J. Anat.* **1966**, *100*, 857.
[21] S. Krauss, W. Wagermaier, J. A. Estevez, J. D. Currey, P. Fratzl, *J. Struct. Biol.* **2011**, *175*, 457.
[22] R. D. Coatman, N. L. Thomas, D. D. Double, *J. Mater. Sci.* **1980**, *15*, 2017.
[23] J. H. Cartwright, B. Escribano, C. I. Sainz-Daz, *Langmuir* **2011**, *27*, 3286.
[24] L. M. Barge, S. S. Cardoso, J. H. Cartwright, G. J. Cooper, L. Cronin, A. De Wit, I. J. Doloboff, B. Escribano, R. E. Goldstein, F. Haudin, D. E. Jones, A. L. Mackay, J. Maselko, J. J. Pagano, J. Pantaleone, M. J. Russell, C. I. Sainz-Diaz, O. Steinbock, D. A. Stone, Y. Tanimoto, N. L. Thomas, *Chem. Rev.* **2015**, *115*, 8652.
[25] S. S. Cardoso, J. H. Cartwright, A. G. Checa, C. I. Sainz-Díaz, *Acta Biomater.* **2016**, *43*, 338.
[26] K. Punia, M. Bucaro, A. Mancuso, C. Cuttitta, A. Marsillo, A. Bykov, W. L'Amoreaux, K. S. Raja, *Langmuir* **2016**, *32*, 8748.
[27] B. C. Batista, P. Cruz, O. Steinbock, *ChemPhysChem* **2015**, *16*, 2299.
[28] L. M. Barge, I. J. Doloboff, L. M. White, G. D. Stucky, M. J. Russell, I. Kanik, *Langmuir* **2012**, *28*, 3714.
[29] K. Kamiya, T. Yoko, K. Tanaka, Y. Fujiyama, *J. Mater. Sci.* **1989**, *24*, 827.
[30] M. Tanahashi, K. Kamiya, T. Suzuki, H. Nasu, *J. Mater. Sci.: Mater. Med.* **1992**, *3*, 48.
[31] C. J. Steenbjerg Ibsen, B. F. Mikladal, U. Bjornholt Jensen, H. Birkedal, *Chem. Eur. J.* **2014**, *20*, 16112.
[32] E. A. Hughes, R. L. Williams, S. C. Cox, L. M. Grover, *Langmuir* **2017**, *33*, 2059.
[33] J. H. Cartwright, J. M. Garcia-Ruiz, M. L. Novella, F. Otalora, *J. Colloid Interface Sci.* **2002**, *256*, 351.
[34] M. Adda-Bedia, S. Kumar, F. Lechenault, S. Moulinet, M. Schillaci, D. Vella, *Langmuir* **2016**, *32*, 4179.
[35] R. Makki, M. Al-Humiari, S. Dutta, O. Steinbock, *Angew. Chem., Int. Ed.* **2009**, *48*, 8752.
[36] G. Tozzi, A. De Mori, A. Oliveira, M. Roldo, *Materials* **2016**, *9*, 267.
[37] Z. Li, Y. Su, B. Xie, H. Wang, T. Wen, C. He, H. Shen, D. Wu, D. Wang, *J. Mater. Chem. B* **2013**, *1*, 1755.
[38] A. Han, G. Rujijanagul, C. Randorn, *Mater. Lett.* **2017**, *193*, 142.
[39] J. Watanabe, M. Kashii, M. Hirao, K. Oka, K. Sugamoto, H. Yoshikawa, M. Akashi, *J. Biomed. Mater Res., Part A* **2007**, *83*, 845.
[40] J. Hu, Y. Zhu, H. Tong, X. Shen, L. Chen, J. Ran, *Int. J. Biol. Macromol.* **2016**, *82*, 134.
[41] L. Cerroni, R. Filocamo, M. Fabbri, C. Piconi, S. Caropreso, S. G. Condò, *Biomol. Eng.* **2002**, *19*, 119.
[42] L. Roszol, O. Steinbock, *Phys. Chem. Chem. Phys.* **2011**, *13*, 20100.
[43] I. Mobasherpour, M. S. Heshajin, A. Kazemzadeh, M. Zakeri, *J. Alloys Compd.* **2007**, *430*, 330.